

Technical Notes



Core Ideas

- Horizontal straight holes for rhizotube installation were bored by a home-made system.
- Dynamics of root growth and soil moisture could be described by rhizotron facilities.
- Soil moisture could be monitored by TDR and GPR approaches in rhizotron facilities.

G. Cai, J. Vanderborght, A. Klotzsche, J. van der Kruk, N. Hermes, and H. Vereecken, Agrosphere, Institute of Bio- and Geosciences (IBG-3), Forschungszentrum Jülich GmbH, Jülich, Germany; J. Neumann, Engineering and Technology, Central Institute for Engineering, Electronics and Analytics (ZEA-1), Forschungszentrum Jülich GmbH, Jülich, Germany. *Corresponding author (g.cai@fz-juelich.de).

Vadose Zone J.
doi:10.2136/vzj2016.05.0043
Received 12 May 2016.
Accepted 13 July 2016.
Supplemental material online.
Open access.

Vol. 15, Iss. 9, 2016
© Soil Science Society of America.
This is an open access article distributed
under the CC BY-NC-ND license
(<http://creativecommons.org/licenses/by-nc-nd/4.0/>).

Construction of Minirhizotron Facilities for Investigating Root Zone Processes

Gaochao Cai,* Jan Vanderborght, Anja Klotzsche, Jan van der Kruk, Joschka Neumann, Normen Hermes, and Harry Vereecken

Minimally invasive monitoring of root development and soil states (soil moisture, temperature) in undisturbed soils during a crop growing cycle is a challenging task. Minirhizotron (MR) tubes offer the possibility to view root development in situ with time. Two MR facilities were constructed in two different soils, stony vs. silty, to monitor root growth, root zone processes, and their dependence on soil water availability. To obtain a representative image of the root distribution, 7-m-long tubes were installed horizontally at 10-, 20-, 40-, 60-, 80-, and 120-cm depths. A homemade system was developed to install MR tubes in the silty soil in horizontally drilled straight holes. For the stony soil, the soil rhizotubes were installed in an excavated and subsequently backfilled pit. In both facilities, three subplots were established with different water treatments: rain sheltered, rainfed, and irrigated. To monitor soil moisture, water potential, and soil temperature, time domain reflectometer probes, tensiometers, and matrix water potential sensors were installed. Soil water content profiles in space and time were obtained between two MR tubes using cross-hole ground-penetrating radar along the tubes at different depths. Results from the first growing season of winter wheat (*Triticum aestivum* L.) after installation demonstrate that differences in root development, soil water, and temperature dynamics can be observed among the different soil types and water treatments. When combined with additional measurements of crop development and transpiration, these data provide key information that is essential to validate and parameterize root development and water uptake models in soil–vegetation–atmosphere transfer models.

Abbreviations: CRIM, complex refraction index model; EMI, electromagnetic induction; GPR, ground-penetrating radar; MR, minirhizotron; SEM, standard error of the sample mean; SWC, soil water content; SWP, soil water potential; TDR, time domain reflectometry; ZOP, zero-offset profile.

A minirhizotron system supplies direct and repeatable views of root morphology in situ in a minimally invasive manner, and it measures responses of root development to various ambient conditions for an extended time period (Johnson et al., 2001). Therefore, the method can be used to investigate the interaction between root development, root senescence, and soil conditions. A typical MR system is composed of a computer, a digital camera, a light source mounted on an index handle, and transparent tubes or rhizotubes installed in the soil at a certain angle.

However, the quality and the representativeness of the root observations made in rhizotubes can be strongly influenced by the method of installation. To ensure high-quality observations, it is generally important to ensure good contact between the soil and the tubes, minimizing or avoiding scratches on the tube surface, and avoiding soil compression. This might be a great challenge in soils with a heavy texture (silt or clay) or with either a stony or coarse texture. For a heavy-textured soil, Hummel et al. (1989) designed a special auger system with combined soil coring bits of which the outer diameters were 2.8% smaller than that of the 30°-angled tubes to ensure a good tube–soil contact while minimizing

soil compaction. The excavation afterward showed that there were generally no gaps, but measurements using a laboratory penetrometer revealed that it caused uniform soil compaction around a tube at a given depth and soil movement along the direction of the tube installation. For a soil with a lot of cobbles and stones, Phillips et al. (2000) used a pneumatic rock drill, which was fixed on a pneumatic screw-drive guide system to make 30°-angled boreholes, and showed that good soil–tube contact was obtained and that there was less soil compaction and disturbance by using this approach in the sandy and rocky soil than using normal techniques (e.g., soil core and auger).

Because of practical reasons, i.e., to avoid the use of heavy machinery, collapse of drilled holes, and tube distortion, MRs are mostly installed either in a vertical manner or with an inclination toward the horizontal surface (vertically inclined). The tubes are usually inclined at 30 or 45°, but other angles are also common in root investigation (Milchunas, 2011; Vamerali et al., 2012). Vertical rhizotubes may lead to artifacts because roots may grow downward preferentially along the tube walls (Bragg et al., 1983). Also for angled tubes, the root density in the surface soil layer was seriously underestimated, whereas in the deeper layers it was overestimated because roots grew, also as a result of gravitropism, preferentially along the soil–tube interface where conditions for growth were more favorable, e.g., lower penetration resistance and moisture droplets on the tubes due to the gaps between the soil and the tubes (De Ruijter et al., 1996; Madi and Kangas, 1997; Stadnyk, 2010). Another problem with vertically inclined MRs is that root observations at a certain depth can be made in only a small surface surrounding the tube. Because of soil heterogeneity and the spatial structure of the root system, a large number of observations or frames are required to obtain a representative estimate of the root density at a certain depth. This implies that a large number of angled tubes are required. Alternatively, a larger number of frames or root observations at a certain depth can be obtained from a horizontally installed MR (Johnson et al., 2001; Smucker, 1993). Furthermore, horizontally installed rhizotubes minimize external influences on the natural soil and the root environment and avoid preferential downward water flows along the soil–tube interface (Eamus, 2006). However, due to the difficulty of horizontal installation, the use of horizontal rhizotubes has been restricted to smaller soil volumes such as lysimeters and outdoor containers (Garré et al., 2011; Meier and Leuschner, 2008) or to large facilities where rhizotubes are installed in repacked soil (Smit et al., 1994; Van de Geijn et al., 1994). Besides, the operation was even more difficult for establishing good contact and minimizing the soil disturbance in extreme soil textures, e.g., stony or clayey soil (Ephrath et al., 1999).

Our objective was to develop a construction procedure for rhizotron facilities with long (7-m) horizontal MRs in a stony and a silty soil. We present here the measurement setup for monitoring the root–root environment using soil moisture, matric potential, and soil temperature sensors as well as ground-penetrating radar (GPR).

Soil sensors typically provide local measurements of soil states; in heterogeneous soils, a large number of sensors may be required to obtain a representative estimate. We obtained data sets from the facility to estimate the spatial variability and the representativeness of the spatial averages of soil moisture and root densities.

Materials and Methods

Field Site

The study site is located in Selhausen (50°52' N, 6°27' E) in Germany and is part of the TERENO Eifel–Lower Rhine observatory (Zacharias et al., 2011). The field is slightly inclined, with a slope of approximately 4°. The main soil in the field is a Luvisol that developed in a layer with a silt loam texture (Weihermüller et al., 2007). The thickness of the silt loam layer varies strongly along the slope of the field. It is up to 3 m thick at the bottom of the slope and not present at the top. This boundary where the sediment layer is present or absent is well indicated by electromagnetic induction (EMI) measurements returning high or low apparent electrical conductivity values, respectively (Rudolph et al., 2015; von Hebel et al., 2014).

The underlying quaternary sediments, which reach to the soil surface at the top of the slope, are fluvial gravel deposits mainly from the Rur river system. The test site is characterized by a strong gradient in stone content, with 60% gravel content in the upper part and approximately 4% in the lower part (Vanderborght et al., 2010). The soil texture is shown in Table 1. One facility was constructed at the top and one at the bottom of the slope. Before the facility was constructed, the field was under a winter barley (*Hordeum vulgare* L.)–winter wheat crop rotation. Winter wheat was sown on 31 Oct. 2014 and harvested on 17 and 31 July 2014 in the upper and lower facilities, respectively.

Setup of Field Plots and Access Trench

Each rhizotron facility was divided into three instrumented plots receiving different water treatments. Each plot was 3.25 m wide

Table 1. Soil texture of the fine soil (<2 mm), mass fraction of stones, field capacity (FC), permanent wilting point (PWP), and porosity in the top- (0–30 cm) and subsoil (30–120 cm) of the upper and lower parts of the field.

Depth	Sand	Silt	Clay	Stone	FC	PWP	Porosity
% —————							
Upper part							
Topsoil†	35	52	13	50	0.15	0.07	0.33
Subsoil††	37	47	16	69	0.09	0.06	0.25
Lower part							
Topsoil†	13	70	17	4	0.37	0.25	0.40
Subsoil†	11	68	21	2	0.29	0.19	0.40

† Soil texture from Weihermüller et al. (2007).

†† Soil texture in the subsoil of the upper part from Stadler et al. (2015).

and 7 m long, and the plots bordered each other along the 7-m-long side. The three plots were bordered by a wooden container (length: 10 m, width: 2.65 m, height: 2.25 m) that was installed in an excavated pit next to the field plots (Fig. 1). The wooden container serves as an access trench with predrilled holes for the rhizotubes and soil moisture sensors. To avoid unwanted reflections in the GPR data, the use of metallic objects in the facilities was avoided as much as possible. To minimize the disturbance of the soil thermal regime by the trench, the facility walls were isolated by 50-mm-thick foam insulation sheets.

One plot was sheltered from rain, one plot was rainfed, and one plot was irrigated with dripper lines. Shelters were installed before the rain started and were removed after the rain stopped. The dripper lines (T-Tape 510-20-500, Wurzelwasser GbR) were installed with 0.3-m intervals and parallel to the access trench. A plastic foil was placed down to 1.3 m at the upper facility to separate the three treatments from each other.

Installation of Rhizotubes

For the installation of the rhizotubes in the upper facility, the high stone content prevented the drilling of horizontal holes (Fig. 1). Instead, a pit of 10 by 10 m was excavated to the 1.3-m depth first. For each plot, three replicate MR tubes, i.e., acrylic glass tubes of 7 m length and with outer and inner diameters of 64 and 56 mm, respectively, were installed at the 10-, 20-, 40-, 60-, 80-, and 120-cm depths with a horizontal offset of 10 cm between tubes at different depth levels so that tubes at a certain depth were not overlain by tubes at other depths (Fig. 2). Root observations at a certain depth are therefore not expected to be influenced by the presence of MRs at other depths. Acrylic glass was used because it has higher hardness (anti-scratch) and transparency and less influence on root growth than other plastics, e.g., butyrate or polycarbonate, and last but not least it is less vulnerable than glass (Withington et al., 2003). The tubes were leveled horizontally on the flattened soil



Fig. 1. Installation of the minirhizotron facility in the upper part of the test site. The wood container is the accessible facility. Wedge-shaped fixture blocks shown in the right corner were used to fix the tubes during soil backfill.

surface using a laser measuring device (Javelin-s, Leica Geosystems) (Fig. 1). To avoid displacement when backfilling the soil, the tubes were fixed by wedge-shaped fixture blocks at three locations and the end was sealed with an inner and an outer cap. The stony soil was carefully backfilled to cover the tubes and sensors. Large stones (>30 mm) were removed when covering the sensors. The backfilled soil was compacted layer by layer to achieve the same bulk density as the undisturbed soil: 1.81 g cm^{-3} in the topsoil layer (0–0.3 m) and 2.02 g cm^{-3} in the subsoil (0.3–1.2 m). The tubes protruded 0.31 m into the access trench to anchor the MR camera. The protruding parts were wrapped in black tape and plugged by opaque caps to prevent light, water, and dust entering the tubes (Fig. 2). A hole with a diameter of 4 mm was drilled on the top side of each tube 0.3 m away from the facility wall. This hole was used to fix the camera system, which consists of an indexing handle that is used to position the camera in the tube, on the rhizotube. By fixing the camera system to the tube and using the indexing handle, images could be repeatedly taken at the same locations along the tube for every measurement.

The design of the facility at the lower part of the slope was similar to that at the upper part (same arrangement of MR tubes, soil sensors, and treatment plots), but the soil below the 20-cm depth was not excavated to install the MR tubes. Instead, the tubes were inserted in horizontally drilled holes. Therefore, a specialized drilling rig was constructed in the Central Institute for Engineering, Electronics and Analytics (ZEA) of Forschungszentrum Jülich (Fig. 3). Steel pipes with an auger inside were pushed into the soil. The pipes were 915 mm long, and the outer and inner diameters were 65 mm and 53 mm, respectively. There was a 50-mm-long drilling bit with a diameter of 20 mm in the front of the auger. The auger, with an outer diameter of 51 mm and a length of 910 mm, was positioned approximately 50 mm out of the pipe (Fig. 3A). Therefore, the drilling unit was used to bore a hole first, and the soil inside the pipe was carried away by the auger. Pipe and auger pieces were screwed together separately with strengthening bolts. The pipes were pushed using

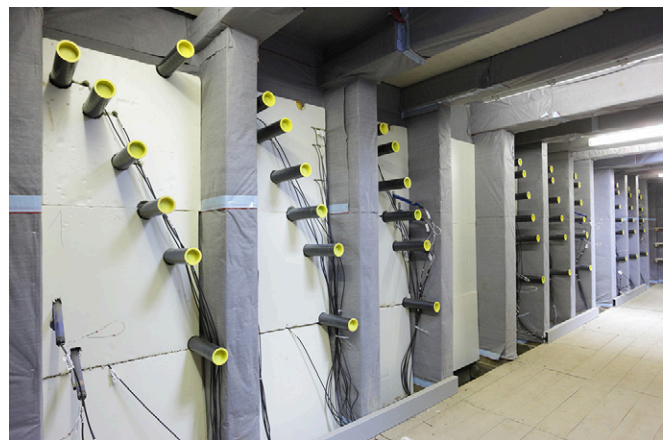


Fig. 2. Interior view of the minirhizotron facility. The rhizotubes were installed perpendicular to the wall profile.

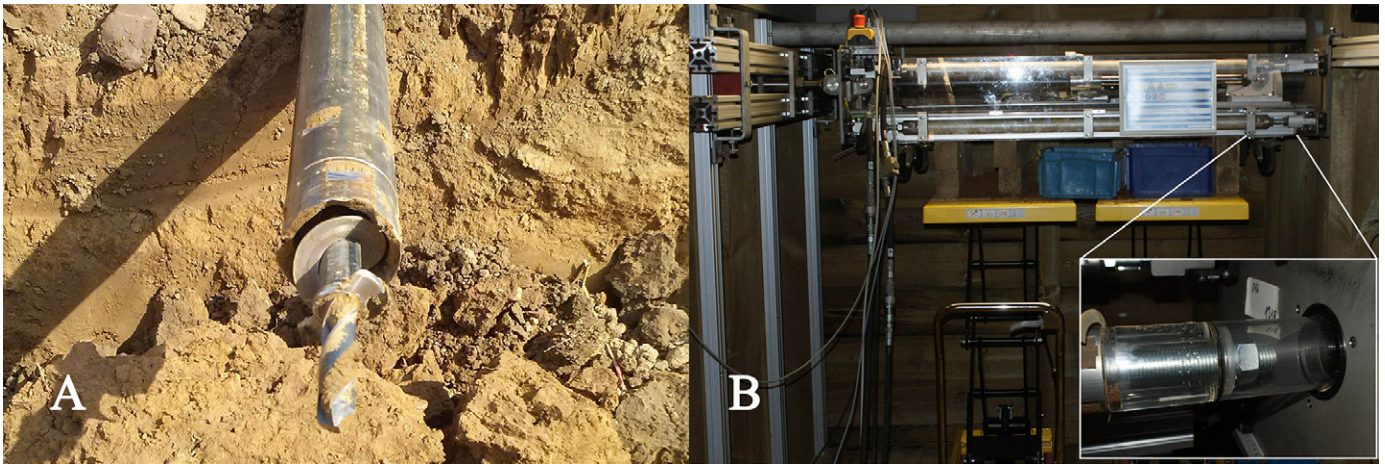


Fig. 3. (A) The steel tube, the auger, and the connected drilling bit; (B) the drilling system for boring horizontal holes and installing the rhizotubes in the lower part of the test site.

a retractable hydraulic cylinder. A maximal force of 127.5 kN could be exerted by the device. The auger rod could withstand a maximal torsion of 190 N m and was connected to other pieces for deeper soil extraction. To keep the direction of the inserted pipes fixed, the drilling rig was suspended in a wheel-equipped frame that was aligned using lasers and fixed to the struts of both sides of the facility (Fig. 3B). The distal ends of the steel tubes deviated at most 5 cm in the horizontal and vertical directions.

When a steel tube of 7-m length was inserted in the soil, a MR was attached to the distal end of the tube. Therefore, a pit was excavated at the other side of the facility where 7-m-long MR tubes could be laid down. A connector that fixed the MR to the steel tube was constructed using a threaded rod and screws so that it could withstand a tensile force of at least 23.9 kN, which corresponds with the tensile strength of the MR. The MR was subsequently pulled back with the steel pipe through the bored hole using the drilling rig, which functioned now as a traction device. Using this procedure, 36 tubes were installed at the 40-, 60-, 80-, and 120-cm depths. Two MR tubes could be installed in 1 d with this technique. The tubes at the 10- and 20-cm depths were installed by excavating the topsoil layer, which is disturbed anyway by soil tillage. A 2.6-m³ water tank was buried in the soil 3 m away from each facility and collected the rainfall from the roof of the wooden container for subsequent irrigation.

Installation and Calibration of Soil Sensors

At each soil depth in each plot, four homemade time-domain reflectometry (TDR) soil moisture sensors (three rods, rod length: 200 mm,

spacing between the rods: 26 mm), one tensiometer (T4e, UMS GmbH), and one MPS-2 matrix water potential and temperature sensor (Decagon Devices) were mounted 0.75 m away from the facility wall. To facilitate the removal of air bubbles in the tensiometers and to improve filling, the tensiometers were installed with an angle of 15° upward. The setup of the rhizotubes and soil sensors in one plot is shown in Fig. 4. In the lower facility, the TDR and MPS-2 sensors were refitted with a round base (Fig. 5) attached to a plastic pipe and were carefully inserted into the predrilled holes from the facility wall. All the sensors in the upper facility and the sensors at 10 and 20 cm in the lower facility were covered by the original soil that was excavated before the installation (Fig. 5).

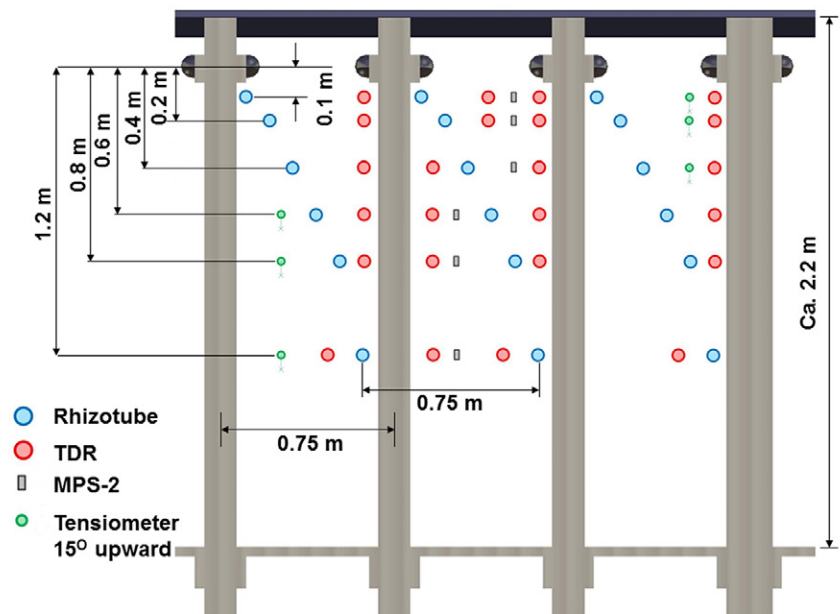


Fig. 4. Setup of the rhizotubes, time-domain reflectometry (TDR) sensors, MPS-2 matrix water potential and temperature sensors, and tensiometers along the transection of the facility wall of one plot.



Fig. 5. Time-domain reflectometry (TDR) sensors in the (A) upper and (B) lower facilities. The bases of the TDR sensors were refitted to a round shape attached to a plastic pipe for inserting into the bored holes in the lower facility.

The soil water content (SWC) and soil water potential (SWP) measured by the sensors in each facility was recorded hourly by two dataloggers (Model CR3000, Campbell Scientific; DT85M, Cosinus Messtechnik GmbH) with multiplexer peripherals, respectively. The multiplexer (50C81-SDM) that connected the TDR probes to the TDR100 cable tester (Campbell Scientific) were constructed with eight different channels. Four cascaded relay levels were used to switch the outer and inner wires of the coaxial cable to make sure that there was no physical connection between different channels during switching and that the travel time of the electromagnetic waves for the eight channels was the same (Weihermüller et al., 2013). This design avoided influences from the electromagnetic noise associated with electrical earth currents, which are present at the site.

For the lower facility in the silty soil, Topp's equation (Topp et al., 1980) was used to calculate the water content from the TDR-measured dielectric permittivity of the soil. Because the soil of the upper facility has a high stone content, a calibration relation between the TDR-measured dielectric permittivity and the SWC was determined in the laboratory. A set of SWCs was established by mixing air-dried soil with a known amount of water. This mixture

was subsequently placed in a container with a known volume and packed to the same bulk density as the field soil. In this container, a TDR probe was installed and the soil was packed around the rods to ensure good contact between the soil and the TDR rods. From the dielectric permittivity that was derived from the TDR waveforms, the water content was calculated using Topp's equation and the complex refraction index model (CRIM) (Herkelrath et al., 1991; Ledieu et al., 1986; Qu et al., 2014).

The relation between the apparent dielectric permittivity measured by TDR and the SWC calculated by Topp's equation and by the CRIM model are shown in Supplemental Fig. S1. The parameters of the CRIM model were obtained by fitting the equation to the SWCs. The SWC was overestimated by Topp's equation in the stony soil. Hence, the fitted CRIM model was used to calculate the SWC from the dielectric permittivity of the stony soil. The calibration was conducted for the top- and subsoil separately, but the relation between the dielectric permittivity and the SWC for the two layers did not differ much, so the same calibration relation was used for both top- and subsoil.

The mean of the SWC measured by the four sensors at a certain depth was calculated. However, the measurements by some sensors deviated considerably from the other sensors at the same depth and water treatments. Therefore, we tested whether certain sensor measurements could be considered as outliers using the Grubbs (1950), Dixon (1950), and median absolute deviation methods (Leys et al., 2013). A description of these tests is given in the supplemental material.

Root Measurements in Rhizotubes

The root development was measured by a minirhizotron system (Bartz Technology Corporation). A digital camera with a visible frame of 13.5 mm (vertical) by 18 mm (horizontal) was used to capture the root images from both the left and right sides of the rhizotubes. The camera was positioned using an indexing handle at 20 observation locations in the tubes. Four series of five locations were taken at 1 to 1.5, 2 to 2.5, 3 to 3.5, and 4 to 4.5 m from the access facility wall. Within a series, the centers of the images were located at 0.04, 0.12, 0.26, 0.38, and 0.5 m from the side of the series (Fig. 6). Repeatable observations could be performed at the same locations with fixed intervals on the index handle. The information on

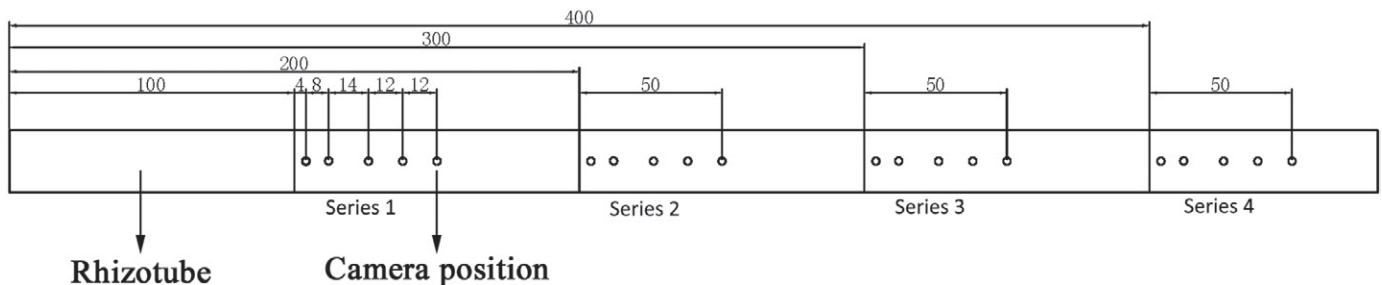


Fig. 6. Measurement locations (circles) distributed in four series along the rhizotube (unit: cm).

rooting depth, root counts, and root length was obtained from the images by using Rootfly (Wells and Birchfield, 2009).

Ground-Penetrating Radar Measurements in Rhizotubes

Ground-penetrating radar is a well-known method to estimate soil water content (Huisman et al., 2003). Two MR tubes can be ideally used to guide a GPR borehole source and receiver to investigate the soil that is present between two MR tubes. The presence of many horizontal MR tubes at different lateral and vertical positions allows a wide range of possible acquisition setups for borehole GPR measurements and a combination with surface GPR measurements to investigate the soil in horizontal and/or (semi)vertical planes. Two borehole measurement methods are possible: a zero-offset profile (ZOP), where the emitting and receiving antenna are located in two different boreholes and simultaneously moved to the next position with a constant spacing between the measurement points; and a multiple-offset gather (MOG), where the transmitter is fixed at several locations in one borehole while the receiver is moved through the whole horizontal borehole for each transmitter location. Multiple-offset gather data enable the reconstruction of detailed two-dimensional images between the two boreholes; however, the measurement time is significantly larger than for ZOP measurements. Due to the many MR tubes, we mainly performed ZOP measurements in horizontal planes every 5 cm between all pairs of neighboring MRs at a given depth (borehole separation of 0.75 m). Because of the presence of the soil sensors and pertaining cables in the first 0.75 m away from the facility wall, GPR measurements were made between 1 and 7 m away from the facility wall. This resulted in a data set covering a soil volume of about 1.2-m depth by 1.5-m width by 6-m length for a certain treatment in a facility. The ZOP measurements were acquired using 200-MHz borehole antennae (PulseEKKO PRO system, Sensors & Software Inc.).

Standard ZOP processing was applied to the data, including correction of time zero, applying a dewow filter to reduce low-frequency noise, and accurate and precise picking of first arrival travel times (Oberrohrmann et al., 2013). Because of interferences of the direct wave in the soil and the critically refracted wave traveling in air, the uppermost shallow ZOP results at the 0.1-m depth cannot be analyzed with a travel-time analysis and were therefore excluded from further analyses. A full-waveform inversion approach is currently in development that includes the full waveforms of both the direct wave and the critically refracted air wave to obtain reliable results for these shallow depths. Recently obtained results of full-waveform inversion approaches for cross-hole GPR in saturated aquifers (Klotzsche et al., 2014) and surface GPR for agricultural soils (Busch et al., 2014) indicate that reliable results can be expected when using such an approach.

Due to the known distance between the MR tubes in which the antennas are located and assuming that the electromagnetic wave is

traveling on a straight path from the transmitting to the receiving antenna, the electromagnetic velocity of the electromagnetic wave can be estimated from the picked travel time. Using an appropriate petrophysical relationship, the measured velocity or dielectric permittivity can be converted into the volumetric water content of the soil, e.g., Steelman and Endres (2011). Similar to the TDR measurements, we used the CRIM model and Topp's equation for the upper and lower facilities, respectively.

Results and Discussion

Installation of Rhizotubes and Sensors

We successfully installed 54 rhizotubes, 72 TDR sensors, 18 tensiometers, and 18 MPS-2 sensors in each facility and then did root measurements weekly as listed in Table 2. In the upper facility, where the tubes were installed in backfilled soil, we didn't observe tube bending or damage 1 yr after installation. This indicates that compaction of the soil to the same density as the undisturbed soil effectively prevented settling and subsidence of the soil, which has been observed to cause tube damage in other studies, e.g., Ephraïm et al. (1999).

For a correct estimate of root distribution, the contact between the tubes and the soil is of great importance and is highly related to the installation procedure. Therefore, we collected 240 images (40 images at each depth \times 6 depths) from the tubes along the soil profile after the upper facility was constructed. The proportion of the void area in the images showed that approximately 92% of the view window was in contact with soil or stones. Phillips et al. (2000) obtained around 89.5% contact in a site with sandy and rocky soil using angled tubes. Because of the high stone content and the irregular shape of the stones, it is impossible to achieve 100% contact between the tubes and the soil. For the lower facility, the borehole was clean and straight because much effort had been made to stabilize the drilling system, and it had a diameter that was 1 mm larger than the diameter of the rhizotube. The images collected after the installation of the rhizotubes showed that the contact between the tubes and the soil was approximately 96%. No obvious soil movement or scratches on the tubes were observed. Because of the good contact between the soil and the rhizotubes,

Table 2. Number of the installed time-domain reflectometry (TDR) sensors, tensiometers, MPS-2 matrix water potential and temperature sensors, and rhizotubes and the measurement frequency of the soil moisture and roots in the two facilities.

Parameter	TDR	Tensiometer	MPS-2	Rhizotube	Images
No. per observation depth of one treated plot in one facility	4	1	1	3	120†
Total number	144	36	36	108	4320
Measurement frequency	1 h ⁻¹	1 h ⁻¹	1 h ⁻¹	1 wk ⁻¹	1 wk ⁻¹

† Images at one observation depth were collected from 40 locations in each of the three replicate rhizotubes.

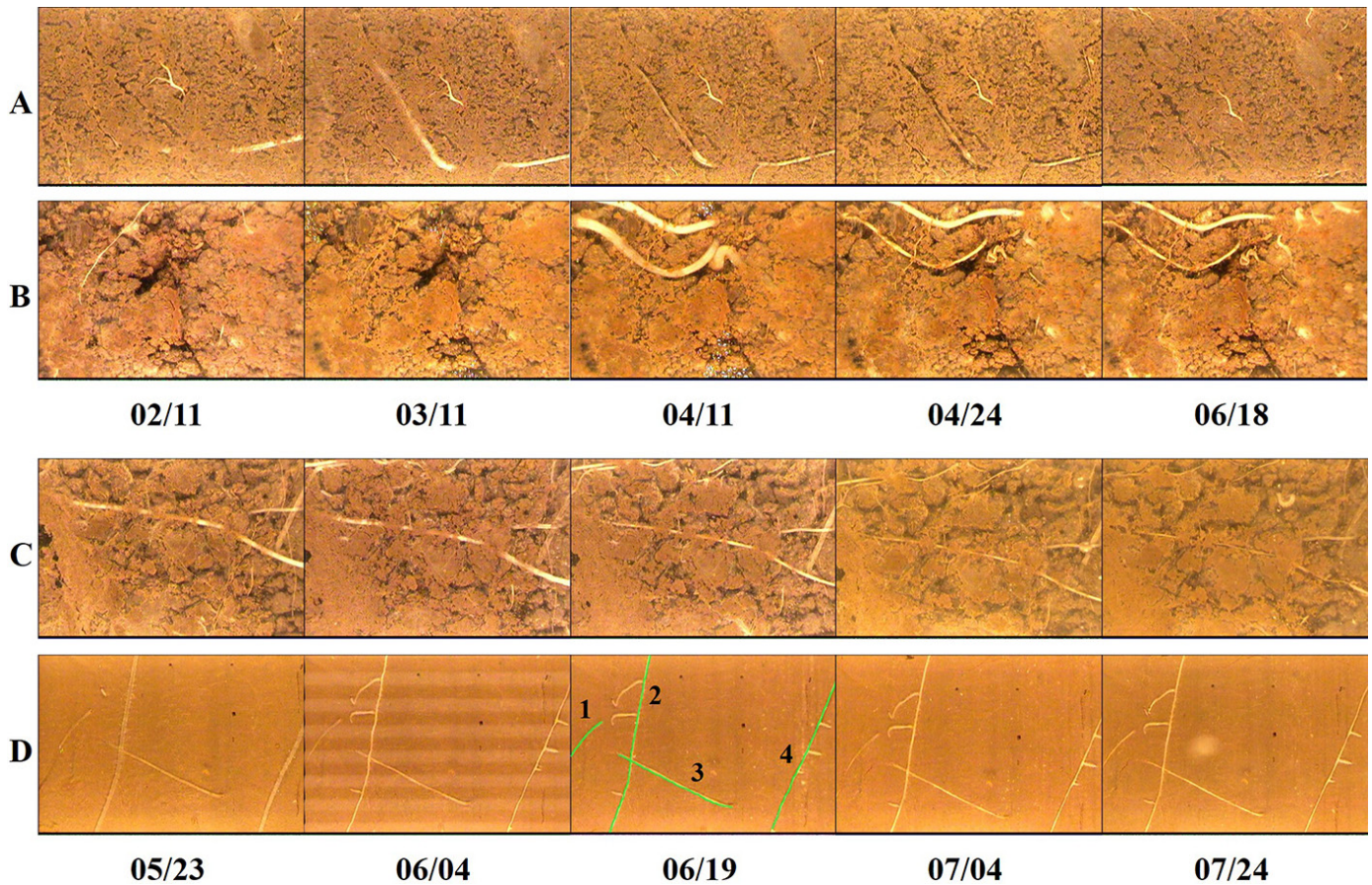


Fig. 7. Time series root images of winter wheat collected from the rhizotubes at (A) 20 cm and (B) 60 cm in the upper facility and at (C) 20 cm and (D) 60 cm in the lower facility. Only single roots were counted and considered in the root analysis but not their laterals. Therefore, there are four roots (green tracks) in the third image of (D).

root clusters and horizontal preferential growth along the tubes were not observed in the root image analysis.

Root Development and Distribution

Figure 7 shows time series of root images of winter wheat that were collected at the same position along the tubes at the 20- and 60-cm depth in the two MR facilities. It clearly illustrates that the appearance, downward development, and senescence of the roots in the top- and subsoil can be recorded with time using the MR system.

The measurements were taken at both left and right sides of the tubes; however, large variations in root counts were observed between the two sides along the tubes at each depth (Fig. 8). For one observation depth and one treatment, roots were counted in 120 13.5- by 18-mm images. This data set represents a sample of the population of all possible root counts at this depth. When the root counts in different images are independent, then the standard deviation (or error) of the sample mean (SEM) can be calculated from the standard deviation of the root counts, σ_{counts} , in the images:

$$\text{SEM} = \frac{\sigma_{\text{counts}}}{\sqrt{N}}$$

where N is the number of images. The number of images that are taken per tube directly relates to the reliability of the root estimation. More images result in higher precision but increase the labor in the subsequent process. However, spatial data such as root counts may be spatially correlated so that root counts

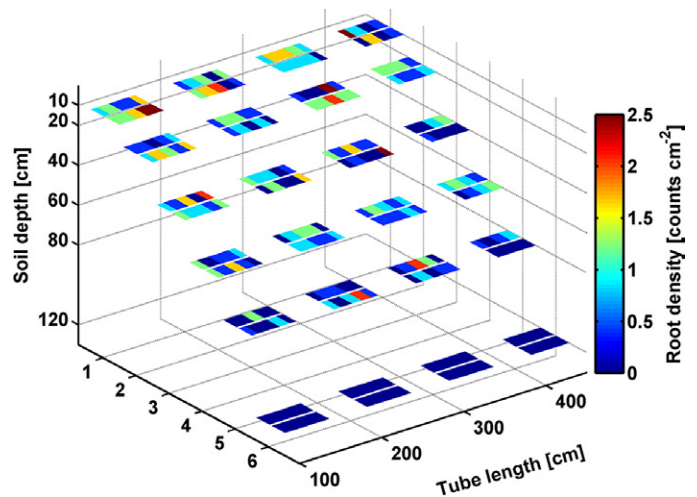


Fig. 8. Root density along the left and right sides of the tubes (one replicate at one soil level) at six soil depths in the rainfed plot of the upper facility. Measurements were taken on 21 May 2014.

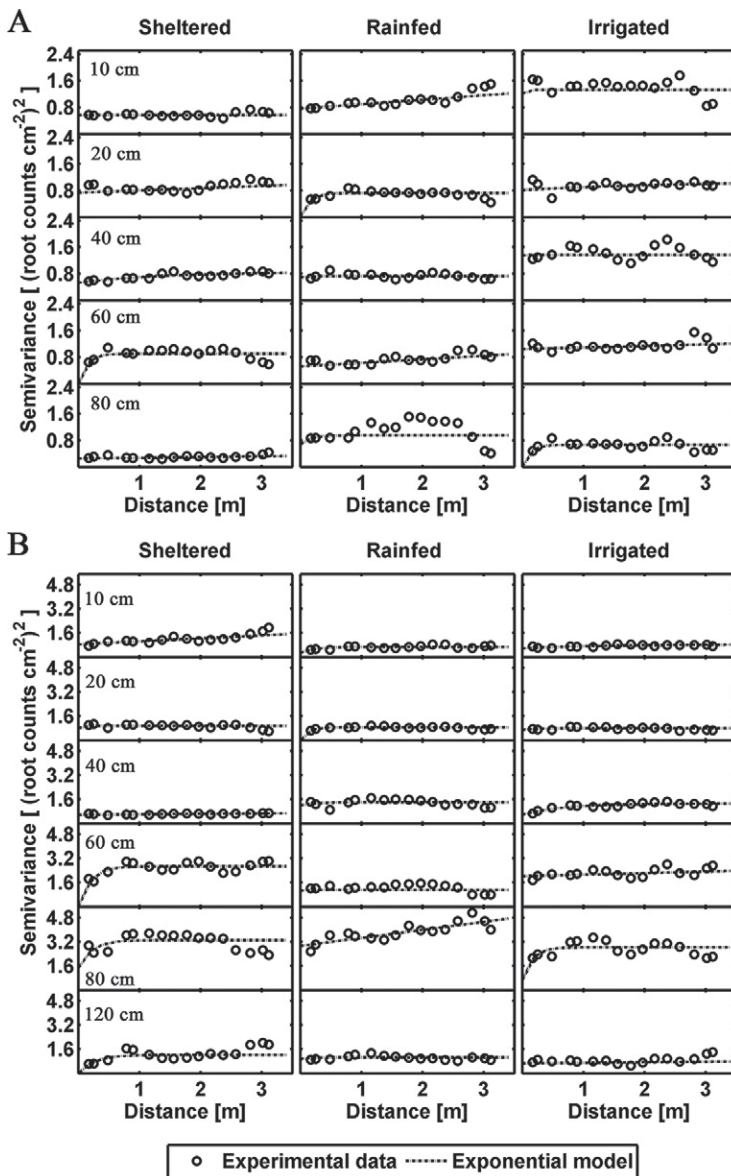


Fig. 9. Variograms for the measured root data in replicate tubes at different soil depths in the (A) upper and (B) lower facilities. Root measurements were taken on 21 and 23 May 2014 for the upper and lower facilities, respectively.

in images that are close to each other are not independent and the precision of the estimate of the mean will not increase when increasing the number of images. For instance, Dubach and Russelle (1995) found that the precision of the mean root counts of alfalfa (*Medicago sativa* L.) was not reduced and a single root was less likely to be counted in more than one image when the number of root images was reduced from 80 to 40 in a horizontal rhizotube. To evaluate the independence of the measurements, we determined the spatial correlation and calculated variograms of the root counts along the tubes as examples on 21 and 23 May for each depth of the three water-treated plots in the two facilities (Fig. 9). For calculation of the variogram, the program Vesper (Minasny et al., 2005) was used.

Eighty percent of the variograms did not show spatial correlations. The intercepts on the y axis were close to the mean variance, which suggested that roots counts in the images were randomly distributed and independent from each other. As a consequence, we calculated the SEM and coefficient of the variation (CV) of the sample mean for the 120 images at each depth in each facility (Fig. 10). The SEM is around $0.06 \text{ counts cm}^{-2}$ in the upper facility, and this corresponds to a CV of the sample mean of 8%. The CV increased to 20% at 80 cm due to fewer roots arriving at this depth. In the lower facility, the SEM was larger and reached up to $0.12 \text{ counts cm}^{-2}$ at the 60- and 80-cm depth. This goes along with the larger root densities at these depths, which were about a factor of two larger than the maximal root densities in the upper facility. The CV is therefore similar to that for the upper facility.

Before discussing the effects of soil texture, observation depth, and water treatment on root densities in detail, we tested the statistical significance of the effect of different factors, such as soil texture, water treatment, and soil depth on root density by an analysis of variance (ANOVA) in MATLAB 8.6.0. A mixed and nested model was set up for the data measured on 21 May 2014 in the upper facility and on 23 May 2014 in the lower facility, so the effect of measurement date was not included in the analysis. Soil texture, water treatment, and soil depth were the fixed factors, whereas the replicated measurement along the horizontal rhizotubes was the random factor, and the random factor was nested to the fixed factors. Root distributions were significantly ($P < 0.001$) influenced by the different soil textures, water treatments, and soil depths (Supplemental Table S1). Overall, the soil texture had the largest effect on the root densities, whereas the water treatment had the smallest effect. The effect of soil depth interacted with that of the soil texture and the water treatment. This implies that in different soil textures, the root distribution with depth varies and the impact of the water treatments is different for different depths. However, no statistically significant interaction between the soil texture and water treatment was observed so that the water treatments apparently had similar effects in the different soil textures. The random nested factor “tube replicate” did not explain a significant part of the variability. This implies that root densities did not differ significantly between replicate tubes, which corroborates with the lack of spatial correlation of root densities.

The spatial and temporal distributions of the root density in the three water-treated plots of the two facilities are shown in Fig. 11. The lower facility was finished 1 yr later than the upper one and the datalogger was ready on 20 May 2014, so the root measurements for this facility are only shown from this date on.

The downward root growth and root development in the beginning of the growth stage could be illustrated for all plots in the upper facility.

For the upper facility, most roots concentrated in the shallow soil from 10 to 40 cm before May. The highest root density appeared at 60 cm in the sheltered and rainfed plots, 40 cm in the irrigated plot. Root density from 10 to 40 cm in the irrigated plot was higher than that in other two plots but decreased significantly with time after the flowering period (21 May). The crops in the irrigated plot ripened earlier (Hossain et al., 2011; Ikeda et al., 1994), and the senescence of the crops resulted in root decay. The maximum observed rooting depths in the three plots were the same, at 80 cm. For the lower facility, roots were detected at the deepest rhizotubes at the 1.2-m depth. The first observations at the lower facility were made on 23 May. After 23 May, root senescence was also observed in the lower facility (except for the 120-cm depth). In contrast to the upper facility, root densities increased with depth until the 80-cm depth (60-cm depth in the irrigated plot), where the highest root densities were observed. At the 80-cm depth, the highest densities were observed in the sheltered plot. The rainfed and irrigated plots showed higher root densities at the 20- and 40-cm depths than the sheltered plot. This could be anticipated based on the higher amount of water that these plots received from rainfall and irrigation than the sheltered plot, leading to drier topsoil conditions in the sheltered plot. The drier upper soil layer in the sheltered plot apparently promoted root development in the deeper soil layers more strongly than in the other plots.

When comparing the lower with the upper facility, the maximum root densities that were observed at 80 cm (60 cm in the irrigated plot) were about twice as high as the maximum root densities that were observed in the upper facility. The higher SWC in the silty deep soil layers of the lower facility may account for the high root density in the deep soil layers (see below). The root densities that were observed in the upper MRs of the lower facility (10–40-cm depth) were, however, similar to their counterparts in the upper facility (around 0.75 counts cm⁻² in the sheltered and rainfed plots and 1.1 counts cm⁻² in the irrigated plot).

Soil Water Content and Water Potential Measurements

The variations in the SWC monitored by TDR sensors at six soil depths in the three water-treated plots of the two facilities are shown from 23 May until 2 August in Fig. 12. The SWC in the lower facility was higher, especially in the subsoil (40 cm and deeper), compared with the corresponding plots of the upper facility, reflecting the difference in stone content and soil texture between the two facilities. Generally, the standard deviation of the SWC in the lower facility was larger than that in the upper one, especially in the deeper soil layers. This may be because soil water movement was quite heterogeneous in the undisturbed silt soil.

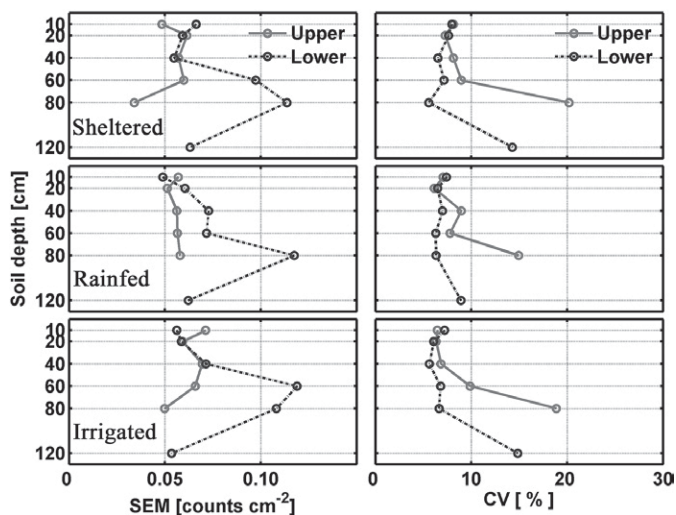


Fig. 10. Standard error of the sample mean (SEM) (left) and the coefficient of the variation (CV) of the sample mean (right) for the measurements from the three replicate tubes ($N = 120$ images) at six observed soil depths in the three water-treated plots of the upper (on 21 May 2014) and lower (on 23 May 2014) facilities.

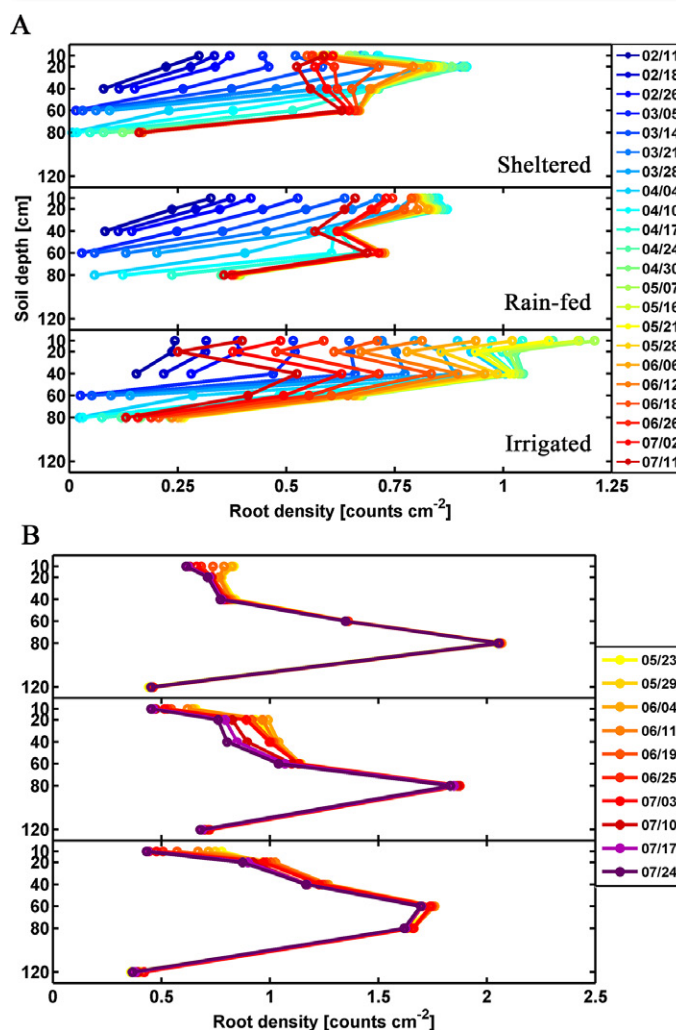


Fig. 11. Time series distributions of root density at six observed soil depths in the sheltered, rainfed, and irrigated plots of the (A) upper and (B) lower facilities.

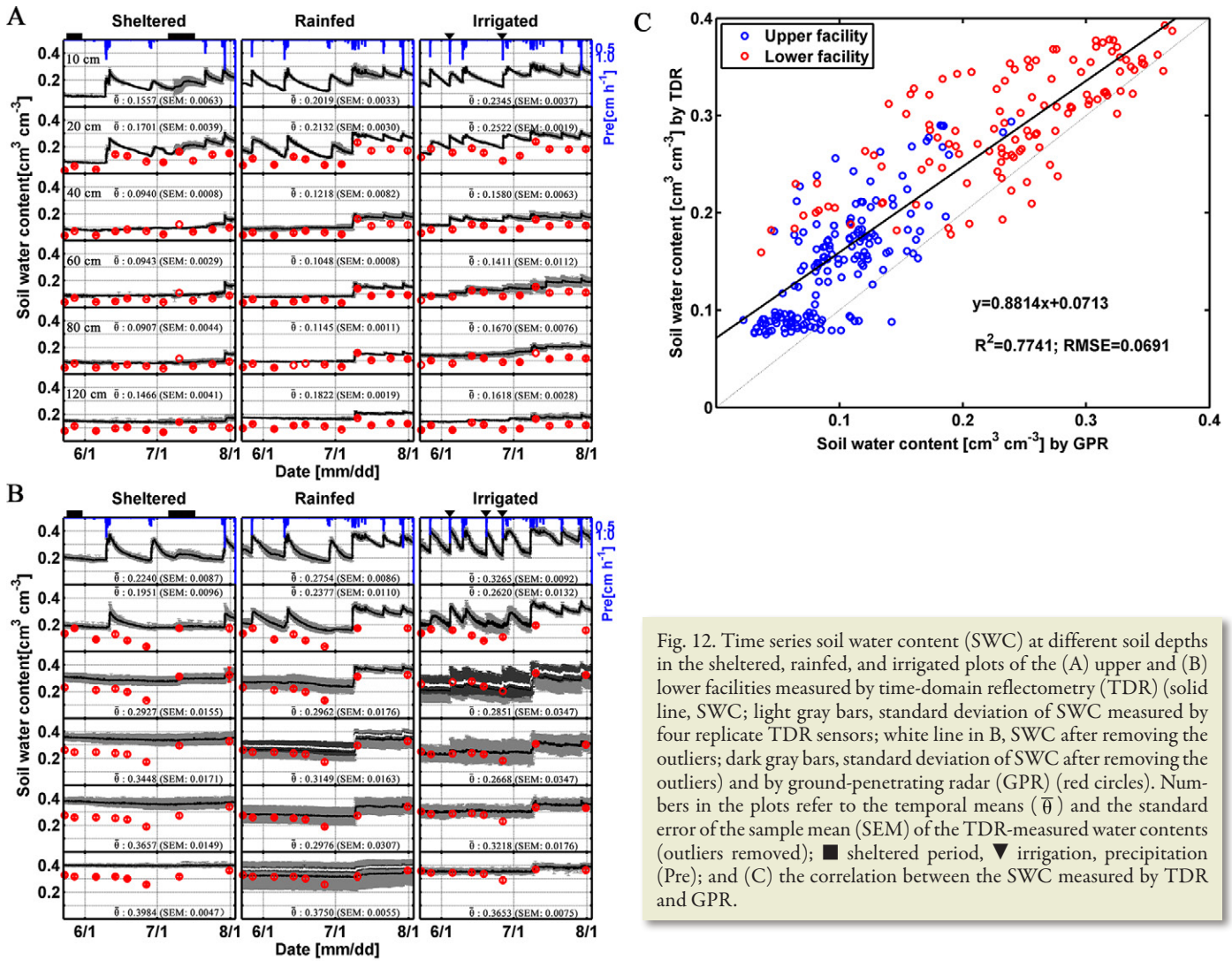


Fig. 12. Time series soil water content (SWC) at different soil depths in the sheltered, rainfed, and irrigated plots of the (A) upper and (B) lower facilities measured by time-domain reflectometry (TDR) (solid line, SWC; light gray bars, standard deviation of SWC measured by four replicate TDR sensors; white line in B, SWC after removing the outliers; dark gray bars, standard deviation of SWC after removing the outliers) and by ground-penetrating radar (GPR) (red circles). Numbers in the plots refer to the temporal means ($\bar{\theta}$) and the standard error of the sample mean (SEM) of the TDR-measured water contents (outliers removed); ■ sheltered period, ▼ irrigation, precipitation (Pre); and (C) the correlation between the SWC measured by TDR and GPR.

Especially the standard deviations of the SWC at 40, 60, 80, and 120 cm in the rainfed plot and at 40 and 60 cm in the irrigated plot of the lower facility were larger than the standard deviations at other depths (Fig. 12B). Therefore, outlier tests were conducted for those depths using Grubbs' approach, as it is usually used for small sample sizes (Supplemental Fig. S2A). The Grubbs' values of 84% of the SWC measurements from suspected sensors at the 60- and 120-cm depths in the rainfed plot and approximately 50% of the values at 40 cm in the irrigated plot were higher than the significance level of 0.05 after 9 July. However, the Grubbs' values at the other three depths were much lower than the critical value, which means that the data were in a reasonable and acceptable range. We also found that the water contents measured by the suspected sensors were 0.1 to 0.2 $\text{cm}^3 \text{cm}^{-3}$ lower than water contents measured by the other sensors. Also, the Dixon and median absolute deviation approaches, which are more robust for smaller sample sizes because they do not use the outlier values to calculate the mean or standard deviation, identified the same suspected sensors as outliers (Supplemental Fig. S2B and S2C). Therefore, the SWCs at those three depths were removed for the subsequent analysis.

When comparing the water contents among different treatments, the time-averaged water contents at the 10- and 20-cm depths decreased, as expected, from the irrigated to the rainfed to the sheltered plots and were higher in the lower than in the upper facility (Fig. 12A and 12B). The temporal variations of soil moisture, especially in the topsoil, responded quickly to the water treatments: increasing values were observed due to irrigation and rainfall and decreasing values because of root water uptake, evaporation, and drainage. For the 40- and 80-cm depths, the water contents were also lower in the unirrigated than in the irrigated plots of the upper facility. For the lower facility, the difference in temporally averaged water contents in the subsoil (40 cm and deeper) among the treatments was not consistent with the different amounts of water that the treatments received. The water content in the subsoil of the irrigated plot was, for instance, lower than that in the sheltered plot even after removing the measurements of the suspected sensor. However, the difference must be compared with the SEM of the four (three when the suspected sensor was removed) soil water sensors, which was larger in the lower facility. Despite the fact that the temporal averages of the water contents in the different plots

of the lower facility could not be linked to the water treatments of the plots, the observed temporal dynamics were consistent with the water treatments. The irrigation and larger rainfall events influenced the dynamics of the soil moisture in the deeper soil layers. In the unirrigated plots, the water contents at 60 cm and deeper soil depths did not respond to the rain events until 9 July, when the rainfall lasted for a week.

The weekly GPR ZOP measurements showed lateral SWC changes along the MR tubes for different depths (not shown). To compare the obtained results with the TDR data, the data were averaged along the 6-m measurements to obtain one mean SWC value for each depth and plotted in Fig. 12 with red circles. Note that the TDR volume of investigation that was within 1 m away from the facility wall could not be sensed by the GPR measurements obtained between 1 and 7 m away from the facility wall due to the interfering reflections of the TDR cables. Despite the fact that TDR and GPR data cannot be compared directly, they show a similar trend but with the GPR SWC being lower (Fig. 12C) than the SWC derived from TDR.

The SWP was monitored both by tensiometers and MPS-2 sensors. Tensiometers are usually used for measuring SWP for wet conditions, whereas MPS-2 sensors are used for drier conditions. The measuring range of the tensiometers and MPS-2 sensors are from 0 to -85 and -9 to -10^5 kPa, respectively (Decagon Devices, 2016; UMS, 2011). The accuracy of the two sensors was ± 0.5 kPa and $\pm(25\%$ of reading $+ 2$ kPa) from -9 to -100 kPa, respectively. The values between -9 and -85 kPa measured by the two types of sensors at different depths were not always correlated as a result of the accuracy of the MPS-2 in this range and the soil heterogeneity. When the water potential continuously decreased to -70 kPa without precipitation or irrigation, the values monitored by the tensiometers leveled off. Therefore, the values between 0 to -70 kPa were chosen from tensiometers, whereas the values lower than -70 kPa were picked from MPS-2 measurements for the subsequent analysis. The temporal variations in SWP in the different plots of the two facilities are shown in Fig. 13. For the topsoil, the SWP in the two facilities increased quickly to a high value (approximately -10 kPa or even higher) after the rain or irrigation events and then decreased subsequently. The decreases in the SWP in this soil layer of the lower facility were larger than those in the upper facility after each precipitation event due to the different soil properties. For the subsoil, the SWP decreased more in the unirrigated plots than in the irrigated plot because less water infiltrated from the topsoil. The SWP at 120 cm, similar to the SWC, was not influenced by the different water treatments. The SWP in the subsoil of the

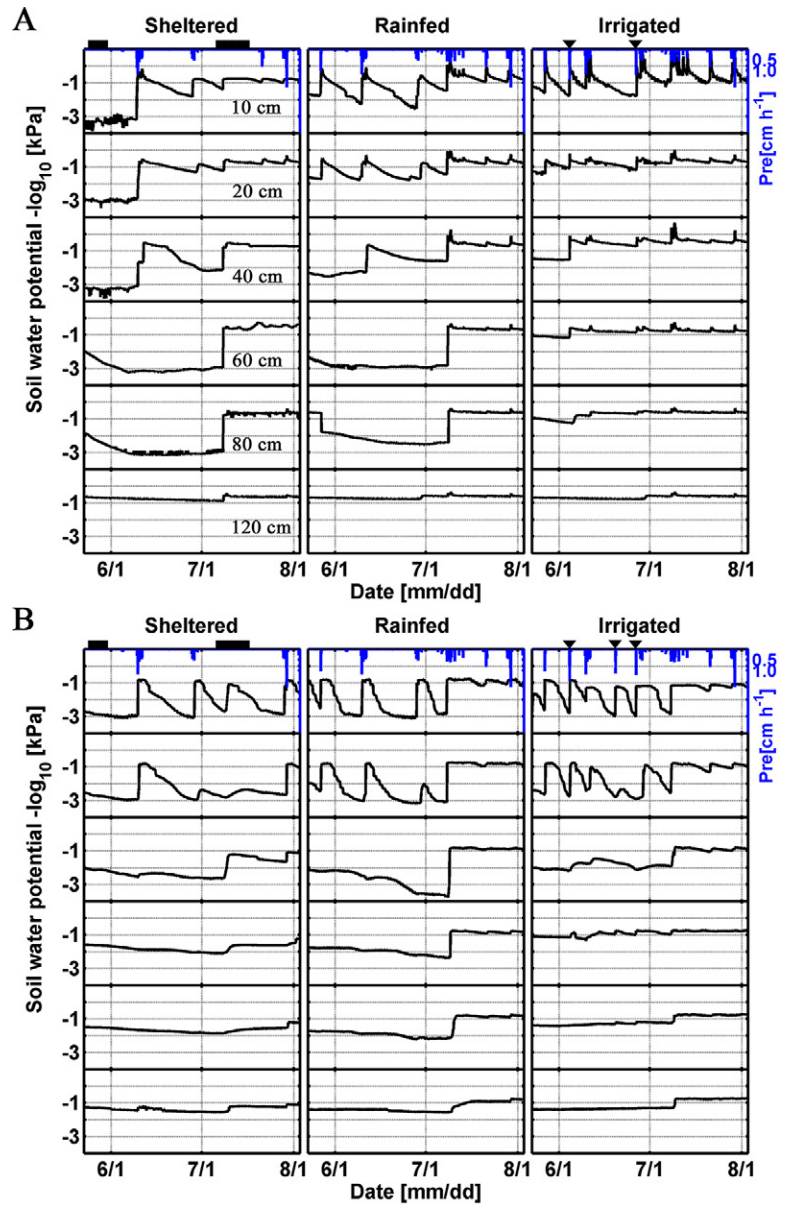


Fig. 13. Time series soil water potential (SWP) at six soil depths in the sheltered, rainfed, and irrigated plots of the (A) upper and (B) lower facilities: sheltered period (■), irrigation (▼), precipitation (Pre).

unirrigated plots in the upper facility decreased to considerably lower values than in the subsoil of the lower facility. This indicates that plants at the lower facility were less subjected to water stress because the water potential in the subsoil, where the root density observed in the MRs was also the largest, was not so low.

Subsequently, the measured SWC and SWP in the three water-treated plots of the two facilities that covered a large range, from near saturated to wilting point, were used to describe the water retention characteristic of the soil. Supplemental Fig. S3A and S3B show the soil water retention curves fitted by the van Genuchten (1980) model for the top- and subsoil of both facilities. The predicted saturated water contents for different soil layers were

generally close to the highest water contents observed in the winter and the periods with frequent rain events. The fitting for the subsoil was not as good as that for the topsoil, which might be mainly due to soil heterogeneity and the smaller range of measured water contents.

Soil Temperature

The spatial and temporal variations of soil temperature at six depths in the three water-treated plots of the two facilities are shown in Supplemental Fig. S4. The soil temperature and the amplitude between daytime and night decreased with increasing soil depths in both facilities. For the upper facility, the soil temperature at each depth of each plot was 1 to 2°C higher than that at the corresponding depths in the lower facility. The high stone content and lower SWC may account for the difference in temperature, although the soil was exposed to the same weather conditions. High stone content changed the soil thermal conductivities and heat capacities (Nobel et al., 1992). Stones or rocks affect the heat in the immediate vicinity of the surrounding soil and act as heat sources at night. Furthermore, the different water treatments had a clear effect on the soil temperature and daily temperature fluctuations in the upper facility, which were larger in the sheltered than in the irrigated plot.

Summary and Conclusions

We constructed two MR facilities to investigate the effect of soil moisture and soil type on the root development of agricultural crops under field conditions. Different soil moisture treatments were established by setting up sheltered, rainfed, and irrigated plots in a stony and in a silty soil. Root development can be monitored in the facilities in horizontally installed rhizotubes at the 10-, 20-, 40-, 60-, 80-, and 120-cm depths. A method to install these rhizotubes without excavating the soil so that the root development can be monitored in naturally structured soil was developed. Besides monitoring root development, the rhizotubes can also be used to map soil water distributions using cross-hole GPR. Also, four TDR sensors were installed in each water–soil treatment to measure soil moisture locally at the depths where the rhizotubes were installed. The local soil measurements within a treatment and depth varied considerably between the different TDR probes and for three out of the 36 soil texture–water treatment–depth combinations; outliers that were identified using statistical outlier detection methods were excluded. The three replicates of 7-m-long rhizotubes that were installed in a soil treatment–depth combination allowed root observations to be obtained at a large number of locations so that differences in root development between different treatments could be tested for statistical significance and spatial correlation. Root density was observed to be larger in the wet treatments and in the silty than in the stony soil. In the silty soil, the highest root densities were observed at the 60- to 80-cm depth but not in the topsoil layer, and the drier treatments showed higher root densities at greater depths than the irrigated treatment. No

spatial correlation of root densities in the horizontal direction was observed for the investigated winter wheat crop, but we anticipate that spatial correlations in root densities in a row crop (e.g., maize [*Zea mays* L.]) could be observed in the rhizotubes.

Plant water stress depends rather on the soil water potentials in the root zone than on the water content. To measure soil water potentials also in the range when soil water potentials create water stress, we installed two types of soil water potential sensors: classical tensiometers that measure water potential to -85 kPa and matrix water potential sensors that can measure to -10^5 kPa. Especially in the upper part of the root zone, very low soil water potentials were measured. To evaluate whether this leads to a reduction in root water uptake, additional measurements that deliver direct or indirect information about the transpiration (e.g., sap flow and canopy surface temperature) are required and planned. It should finally be noted that soil temperatures were higher in drier treatments. To what extent this can be related to different soil thermal properties of the drier soil or to a smaller transpiration and hence smaller evaporative cooling requires further investigation.

Acknowledgments

We acknowledge the financial support of SFB/TR 32 (Transregional Collaborative Research Centre 32) funded by the Deutsche Forschungsgemeinschaft (DFG). We thank Rainer Harms, Stefanie Pickel, Werner Küpper, Martina Kettler, and Bernhard Peter Roland, Garten- und Landschaftsbau, for providing much effort for installing the facilities. We are grateful to Odilia Esser, Max Oberrohrmann, Katrin Huber, Betiglu Abesha, and Matthias Kelter for their help. We also thank the TEREÑO project for providing the data on precipitation and air temperature.

References

- Bragg, P., G. Govi, and R. Cannell. 1983. A comparison of methods, including angled and vertical minirhizotrons, for studying root growth and distribution in a spring oat crop. *Plant Soil* 73:435–440. doi:10.1007/BF02184322
- Busch, S., J. van der Kruk, and H. Vereecken. 2014. Improved characterization of fine-texture soils using on-ground GPR full-waveform inversion. *IEEE Trans. Geosci. Remote Sens.* 52:3947–3958.
- Decagon Devices. 2016. MPS-2 & MPS-6 dielectric water potential sensors operator's manual. Decagon Devices, Pullman, WA.
- De Ruijter, F., B. Veen, and M. Van Oijen. 1996. A comparison of soil core sampling and minirhizotrons to quantify root development of field-grown potatoes. *Plant Soil* 182:301–312. doi:10.1007/BF00029061
- Dixon, W.J. 1950. Analysis of extreme values. *Ann. Math. Stat.* 21:488–506. doi:10.1214/aoms/1177729747
- Dubach, M., and M.P. Russelle. 1995. Reducing the cost of estimating root turnover with horizontally installed minirhizotrons. *Agron. J.* 87:258–263. doi:10.2134/agronj1995.00021962008700020019x
- Eamus, D. 2006. *Ecohydrology: Vegetation function, water and resource management*. CSIRO, Collingwood, VIC, Australia.
- Ephrath, J., M. Silberbush, and P. Berliner. 1999. Calibration of minirhizotron readings against root length density data obtained from soil cores. *Plant Soil* 209:201–208. doi:10.1023/A:1004556100253
- Garré, S., M. Javaux, J. Vanderborght, and H. Vereecken. 2011. Three-dimensional electrical resistivity tomography to monitor root zone water dynamics. *Vadose Zone J.* 10:412–424. doi:10.2136/vzj2010.0079
- Grubbs, F.E. 1950. Sample criteria for testing outlying observations. *Ann. Math. Stat.* 21:27–58. doi:10.1214/aoms/1177729885
- Herkelrath, W., S. Hamburg, and F. Murphy. 1991. Automatic, real-time monitoring of soil moisture in a remote field area with time domain reflectometry. *Water Resour. Res.* 27:857–864. doi:10.1029/91WR00311
- Hossain, M.A., H. Araki, and T. Takahashi. 2011. Poor grain filling induced by waterlogging is similar to that in abnormal early ripening in wheat in western Japan. *Field Crops Res.* 123:100–108. doi:10.1016/j.fcr.2011.05.005

- Huisman, J., S. Hubbard, J. Redman, and A. Annan. 2003. Measuring soil water content with ground penetrating radar. *Vadose Zone J.* 2:476–491. doi:10.2136/vzj2003.4760
- Hummel, J., M. Levan, and K. Sudduth. 1989. Minirhizotron installation in heavy soils. *Trans. ASAE* 32:770–776. doi:10.13031/2013.31067
- Ikeda, K., T. Kume, H. Tabuo, N. Yoshida, and S. Izumi. 1994. Occurrence of abnormal early ripening of wheat and its control in Kagoshima prefecture [Japan]: 2. Root activity of wheat in infected soil. *Kyushu Okinawa Agric. Res. Ctr., Kumamoto, Japan.*
- Johnson, M., D. Tingey, D. Phillips, and M. Storm. 2001. Advancing fine root research with minirhizotrons. *Environ. Exp. Bot.* 45:263–289. doi:10.1016/S0098-8472(01)00077-6
- Klotzsche, A., J. van der Kruk, J. Bradford, and H. Vereecken. 2014. Detection of spatially limited high-porosity layers using crosshole GPR signal analysis and full-waveform inversion. *Water Resour. Res.* 50:6966–6985. doi:10.1002/2013WR015177
- Ledieu, J., P. De Ridder, P. De Clerck, and S. Dautrebande. 1986. A method of measuring soil moisture by time-domain reflectometry. *J. Hydrol.* 88:319–328. doi:10.1016/0022-1694(86)90097-1
- Leys, C., C. Ley, O. Klein, P. Bernard, and L. Licata. 2013. Detecting outliers: Do not use standard deviation around the mean, use absolute deviation around the median. *J. Exp. Soc. Psychol.* 49:764–766. doi:10.1016/j.jesp.2013.03.013
- Madi, H., and P. Kangas. 1997. Demography of fine roots in response to nutrient applications in a Norway spruce stand in southwestern Sweden. *Ecoscience* 4:199–205.
- Meier, I.C., and C. Leuschner. 2008. Genotypic variation and phenotypic plasticity in the drought response of fine roots of European beech. *Tree Physiol.* 28:297–309. doi:10.1093/treephys/28.2.297
- Milchunas, D.G. 2011. Potential biases, problems, and advantages of minirhizotron. In: S. Mancuso, editor, *Measuring roots: An updated approach*. Springer, Berlin, p. 316.
- Minasny, B., A.B. McBratney, and B.M. Whelan. 2005. VESPER version 1.62. *Aust. Ctr. Precis. Agric., Univ. of Sydney, NSW, Australia.*
- Nobel, P.S., P.M. Miller, and E.A. Graham. 1992. Influence of rocks on soil temperature, soil water potential, and rooting patterns for desert succulents. *Oecologia* 92:90–96. doi:10.1007/BF00317267
- Oberröhrmann, M., A. Klotzsche, H. Vereecken, and J. van der Kruk. 2013. Optimization of acquisition setup for cross-hole GPR full-waveform inversion using checkerboard analysis. *Near Surf. Geophys.* 11:197–209. doi:10.3997/1873-0604.2012045
- Phillips, D.L., M.G. Johnson, D.T. Tingey, C. Biggart, R.S. Nowak, and J.C. Newsom. 2000. Minirhizotron installation in sandy, rocky soils with minimal soil disturbance. *Soil Sci. Soc. Am. J.* 64:761–764. doi:10.2136/sssaj2000.642761x
- Qu, W., H. Bogen, J.A. Huisman, G. Martinez, Y.A. Pachepsky, and H. Vereecken. 2014. Effects of soil hydraulic properties on the spatial variability of soil water content: Evidence from sensor network data and inverse modeling. *Vadose Zone J.* 13(12). doi:10.2136/vzj2014.07.0099
- Rudolph, S., J. van der Kruk, C. von Hebel, M. Ali, M. Herbst, C. Montzka, et al. 2015. Linking satellite derived LAI patterns with subsoil heterogeneity using large-scale ground-based electromagnetic induction measurements. *Geoderma* 241–242:262–271. doi:10.1016/j.geoderma.2014.11.015
- Smit, A., J. Groenwold, and J. Vos. 1994. The Wageningen Rhizolab: A facility to study soil–root–shoot–atmosphere interactions in crops. *Plant Soil* 161:289–298. doi:10.1007/BF00046400
- Smucker, A. 1993. Soil environmental modifications of root dynamics and measurement. *Annu. Rev. Phytopathol.* 31:191–218. doi:10.1146/annurev.py.31.090193.001203
- Stadler, A., S. Rudolph, M. Kupisch, M. Langensiepen, J. van der Kruk, and F. Ewert. 2015. Quantifying the effects of soil variability on crop growth using apparent soil electrical conductivity measurements. *Eur. J. Agron.* 64:8–20. doi:10.1016/j.eja.2014.12.004
- Stadnyk, C.N. 2010. Root dynamics and carbon accumulation of six willow clones in Saskatchewan. M.S. thesis. Univ. of Saskatchewan, Saskatchewan, SK, Canada.
- Steelman, C.M., and A.L. Endres. 2011. Comparison of petrophysical relationships for soil moisture estimation using GPR ground waves. *Vadose Zone J.* 10:270–285. doi:10.2136/vzj2010.0040
- Topp, G., J. Davis, and A.P. Annan. 1980. Electromagnetic determination of soil water content: Measurements in coaxial transmission lines. *Water Resour. Res.* 16:574–582. doi:10.1029/WR016i003p00574
- UMS. 2011. Pressure transducer tensiometer T4/T4e: User manual. UMS, München, Germany.
- Vameralli, T., M. Bandiera, and G. Mosca. 2012. Minirhizotrons in modern root studies. In: S. Mancuso, editor, *Measuring roots: An updated approach*. Springer, Berlin, p. 341–361. doi:10.1007/978-3-642-22067-8_17
- Van de Geijn, S., J. Vos, J. Groenwold, J. Goudriaan, and P. Leffelaar. 1994. The Wageningen Rhizolab: A facility to study soil–root–shoot–atmosphere interactions in crops. *Plant Soil* 161:275–287. doi:10.1007/BF00046399
- Vanderborght, J., A. Graf, C. Steenpass, B. Scharnagl, N. Prolingheuer, M. Herbst, et al. 2010. Within-field variability of bare soil evaporation derived from eddy covariance measurements. *Vadose Zone J.* 9:943–954. doi:10.2136/vzj2009.0159
- van Genuchten, M.Th. 1980. A closed-form equation for predicting the hydraulic conductivity of unsaturated soils. *Soil Sci. Soc. Am. J.* 44:892–898. doi:10.2136/sssaj1980.03615995004400050002x
- von Hebel, C., S. Rudolph, A. Mester, J.A. Huisman, P. Kumbhar, H. Vereecken, and J. van der Kruk. 2014. Three-dimensional imaging of subsurface structural patterns using quantitative large-scale multi-configuration electromagnetic induction data. *Water Resour. Res.* 50:2732–2748. doi:10.1002/2013WR014864
- Weiherrmüller, L., J.A. Huisman, N. Hermes, S. Pickel, and H. Vereecken. 2013. A new TDR multiplexing system for reliable electrical conductivity and soil water content measurements. *Vadose Zone J.* 12(2).
- Weiherrmüller, L., J. Huisman, S. Lambot, M. Herbst, and H. Vereecken. 2007. Mapping the spatial variation of soil water content at the field scale with different ground penetrating radar techniques. *J. Hydrol.* 340:205–216. doi:10.1016/j.jhydrol.2007.04.013
- Wells, C., and S. Birchfield. 2009. *Rootfly: Software for minirhizotron image analysis*. College Eng., Comput., Appl. Sci., Clemson Univ., Clemson, SC.
- Withington, J.M., A.D. Elkin, B. Buřaj, J. Olesiński, K.N. Tracy, T.J. Bouma, et al. 2003. The impact of material used for minirhizotron tubes for root research. *New Phytol.* 160:533–544. doi:10.1046/j.1469-8137.2003.00903.x
- Zacharias, S., H. Bogen, L. Samaniego, M. Mauder, R. Fuß, T. Pütz, et al. 2011. A network of terrestrial environmental observatories in Germany. *Vadose Zone J.* 10:955–973. doi:10.2136/vzj2010.0139